https://doi.org/10.5194/amt-2022-278
Preprint. Discussion started: 4 November 2022

Atmospheric Measurement Techniques Discussions

Performance evaluation of portable dual-spot micro-aethalometers for source identification of Black Carbon aerosols: Application to wildfire smoke and traffic emissions in the Pacific Northwest

Mrinmoy Chakraborty[1], Amanda Giang[1,2], and Naomi Zimmerman[1]

[1]Department of Mechanical Engineering, University of British Columbia, Vancouver, Canada, V6T 1Z4
[2]Institute for Resources, Environment and Sustainability, University of British Columbia, Vancouver, Canada, V6T 1Z4

Correspondence: Naomi Zimmerman (nzimmerman@mech.ubc.ca)

Abstract. Black Carbon (BC) is a component of particulate matter, emitted from the incomplete combustion of carbonaceous fuels. The presence of BC in the atmosphere can disrupt the atmospheric radiation budget, and exposure to BC can adversely affect human health. Multi-wavelength light absorption-based dual-spot aethalometers can be used to quantify the source and characteristics of BC from traffic or biomass burning-based sources. However, aethalometer measurements are affected by artifacts such as aerosol loading and light scattering; hence, they often need correction to reduce measurement uncertainty. This work assesses the performance of the recently developed portable aethalometer (MA300, AethLabs). Due to their portability and ease of usage, MA300s can be suitable for mobile and personal exposure monitoring. Here, we evaluate BC concentration and source apportionment accuracy of three MA300 units relative to a widely used aethalometer, the AE33 (Magee Scientific). Synchronous field measurements were performed at a major traffic intersection during regular and wildfire smoke-affected days in Vancouver, Canada. We find that MA300 reported BC mass concentrations were strongly correlated (Slope range between 0.73 and 1.01, with R^2 = 0.9) compared to the reference instrument, yet there is visible instrumental variability (15%) across three units. The mean absolute error of MA300 reported BC concentrations ranged between 0.44–0.98 $\mu g\,m^{-3}$ with the highest deviations observed in wildfire smoke-affected polluted days. From the aerosol light absorption measurement perspective, MA300s tend to underestimate the absorption coefficients (b_{abs}) across the five wavelengths. UV channel light absorption results were subjected to the highest amount of noise, leading to systematic bias in source apportionment analysis. We investigated the application of the latest non-linear aethalometer correction protocols in the MA300 and found that flow fluctuations enhanced noise across all channels, compared to onboard instrument correction. We also identify that the UV ($\lambda = 370$ nm) channel absorption measurements are most sensitive to instrumental artifacts during the wildfire smoke-affected period. Hence, as an alternative to traditional UV and IR ($\lambda = 880$ nm)-based BC source apportionment methods, in this work, we tested the Blue ($\lambda = 470$ nm) and IR wavelengths for BC source apportionment calculation. By adopting Blue-IR based source apportionment technique in MA300, the apportioned BC components improves on average in the order of 10% when compared against the reference monitor's results.

https://doi.org/10.5194/amt-2022-278
Preprint. Discussion started: 4 November 2022

Atmospheric Measurement Techniques Discussions

1 Introduction

Black Carbon (BC) is the major light absorbing component of atmospheric aerosol, produced from the incomplete combustion or pyrolysis of carbonaceous matter (Bond and Bergstrom, 2006). During the past decade, there has been significant interest in BC as a key research target for climate change and health impact assessment studies (Petzold et al., 2013), as BC has been identified as a short-lived climate forcer (Szopa et al., 2021) and its mitigation strategies can contribute to achieving near-term climate goals. Additionally, the World Health Organization recognized BC as one of the primary causes of cardiopulmonary morbidity and mortality as it may act as a universal carrier of chemicals of varying toxicity to the lungs.(WHO, 2012) Yet, accurate real-time monitoring of BC concentration and quantitative source attribution in different macro and micro-environments remains a challenge due to the presence of measurement artifacts, logistical issues (for example, remote sampling locations with limited access to electricity), and lack of clear scientific assessments of instrument performance.(Alas et al., 2020; Segura et al., 2014)

Measurement of BC is a complicated process because there is no clear chemical definition of the species(Tasoglou et al., 2018). BC particles, composed primarily of graphene-like sp2-bonded carbon and refractory in nature, strongly absorb short- and long-wave light radiation (Lack et al., 2014). Several measurement techniques have been developed based on these observed properties of BC, and the definition of BC can change based on the technique adopted. Traditionally, the mass concentration of BC has been quantified by two processes: (1) as elemental carbon (EC) mass concentration derived from thermal-optical analysis of aerosol deposited on filters (Bauer et al., 2009)(e.g. Sunset thermal-optical OC-EC analyzer) and (2) as equivalent black carbon (eBC) measurements derived from light absorption of aerosol collected on a filter (Hansen et al., 1984) material (e.g. Aethalometer, Multi-Angle Absorption Photometer) or from photo-acoustic measurements (e.g. the Photo Acoustic Soot Spectrometer). More recently, the laser-induced incandescence (LII) technique has been used to measure refractory BC (rBC) concentration after the development of the Single Particle Soot Photometer (SP2) instrument (Schwarz et al., 2006). From the pool of commercially-available instruments, aethalometers have been extensively used by the scientific community and regulatory bodies to monitor real-time BC (or eBC) concentration; however, few studies have compared and reported the benefits and measurement uncertainties of the different BC measuring instruments used in the literature (Petzold et al., 2013; Tasoglou et al., 2018).

In aethalometers, aerosol particles are collected on filter tape by drawing sample air from the environment; synchronous light transmission measurements are then performed by photometers (Hansen et al., 1984). Light transmission measurements are converted to attenuation (ATN) units, and the rate of change of ATN is converted to BC mass concentration. The aethalometer reported BC mass concentrations are derived from the light absorption measurements at an infrared (IR) wavelength (880 nm), as light absorption at 880 nm has been identified as being due to pure BC only (Hansen et al., 1984). Combustion-generated light-absorbing aerosol components interact differently with light at different wavelengths based on the source/type of fuel or combustion temperature. Combustion of wood leads to both BC and light-absorbing organic compounds (e.g. polycyclic aromatic hydrocarbons or humic-like substances), which tend to absorb light at lower wavelengths strongly (e.g., UV $\sim$ 365 nm) (Sandradewi et al., 2008a). Fossil-fuel-based aerosol sources (e.g., diesel vehicles) generate aerosol, which tends to absorb

https://doi.org/10.5194/amt-2022-278
Preprint. Discussion started: 4 November 2022


Atmospheric Measurement Techniques Discussions

light uniformly across the spectrum (Bond and Bergstrom, 2006). Based on these developments, recent aethalometers are equipped with multi-wavelength (UV to IR) light absorption capabilities, which have been used for source characterization of BC (Sandradewi et al., 2008b; Helin et al., 2018; Healy et al., 2017).

Aethalometer-reported raw BC measurements often require additional complex corrections applied to the light absorption data to account for measurement artifacts from the filter loading effect and the multiple scattering effect (Drinovec et al., 2015; Virkkula et al., 2007; Weingartner et al., 2003). As particle deposition on the filter spot increases, the newer particle deposits are subject to a shadowing effect (i.e., loading effect) on the light transmission, resulting in a non-linear change of ATN with BC concentration at the higher ATN range (Weingartner et al., 2003; Gundel et al., 1984). To account for the loading effect, a compensation scheme is usually embedded in the aethalometer software by assuming fixed compensation parameters (Virkkula et al., 2007, 2015) or by considering the dynamic changes in the aerosol loading (Drinovec et al., 2015). In addition to the loading effect, aerosol components may scatter light (depending upon aerosol composition, e.g. presence of salt components), and light scattered from the filter media can also impact the aethalometer light ATN measurements. This effect is typically corrected by incorporating a multiple-scattering correction factor (C) within the aethalometer correction mechanism. Studies have determined the value of C by comparing measurements from different instruments in laboratories and field (Weingartner et al., 2003; Segura et al., 2014; Bernardoni et al., 2021), and reported that C strongly depends on the filter material used (e.g. $C_{quartz} = 2.14$ and $C_{TFE} = 1.57$)(Drinovec et al., 2015).

The Magee Scientific AE33 aethalometer measures aerosol light absorption at seven different wavelengths (370-950 nm) and uses the latest dual-spot technique to measure real-time BC concentration (Drinovec et al., 2015; Rajesh and Ramachandran, 2018). Dual-spot aethalometers use two deferentially loaded filter spots to estimate real-time light attenuation measurement with respect to a reference (or clean) spot. AE33s have been extensively used in recent field studies around the world (Cuesta-Mosquera et al., 2021; Duc et al., 2020; Goel et al., 2021; Li et al., 2020; Wang et al., 2021) and are considered a reference-grade instrument for accurate and real-time measurement of BC (or equivalent BC) (Bernardoni et al., 2021; Healy et al., 2017; Meena et al., 2021; Rajesh et al., 2021). Data collected from AE33s have also been used to provide insights into aerosol light absorption and to identify BC sources (biomass burning or traffic emission) based on the widely-used two-component aethalometer model (Sandradewi et al., 2008a; Healy et al., 2017; Rajesh et al., 2021). Source apportionment of BC aerosol from the two-component aethalometer model divides the BC concentration into two segments based on their source of origin (biomass burning or fossil fuel-based sources). Near-UV and near-IR light absorption measurements estimate the two BC source fractions. However, the choice of wavelength can change the estimates and has been extensively studied in literature (Zotter et al., 2017).

Although advanced aethalometers like the AE33 are widely used, they may not be appropriate in certain environments where portability and battery-powered operation are essential since these instruments are typically expensive, bulky, and require external pumps or an external power supply to operate. Portable but effective instruments are often required for mobile monitoring, in-vehicle commuter exposure (Weichenthal et al., 2015; Apte et al., 2011), indoor personal exposure (Jeong and Park, 2017), and for monitoring wildfire smoke using unmanned aerial vehicles.(Aurell et al., 2021) Over the past decade, researchers have become increasingly interested in micro-aethalometers, as they are suitable for characterizing emissions in these challenging

https://doi.org/10.5194/amt-2022-278
Preprint. Discussion started: 4 November 2022


Atmospheric Measurement Techniques Discussions

micro-environments (Alas et al., 2020; Aurell et al., 2021; Liu et al., 2021). The newly developed micro-aethalometer model MA300 (AethLabs) uses similar measurement techniques to the AE33 but with a smaller form factor, a built-in rechargeable battery, and a low-volume pump, making it suitable for indoor measurements and personal exposure analysis.

With the potential for increased use of the MA300 in the scientific community or by regulatory bodies, it is critical to evaluate the real-world performance of the MA300 against reference instruments with regards to BC mass concentration, aerosol light absorption measurements and source characterization capabilities. Such evaluation requires a real-world assessment of the onboard MA300 correction mechanism and exploration of opportunities for improved methods. Currently, the MA300's onboard correction algorithm utilizes a linear correction method (Virkkula et al., 2007) applied on simultaneous dual filter spot (dual-spot) measurements. This method does not consider the non-linearity arising from flow and may lead to the underestimation of BC in higher ATN ranges. The AE33 onboard algorithm, in contrast, uses a real-time non-linear dual-spot correction, including adjustments for variable flow rate (Drinovec et al., 2015).

In this work, we compare three MA300 units and their performance with a reference AE33 instrument through a long-term co-location campaign in Vancouver, Canada. During the campaign, all aethalometers were exposed to daily traffic emissions from the nearby multi-lane major road intersection as well as several days of wildfire smoke. In recent years, frequent wildfires in the Pacific Northwest regions of North America have been contributing to an increasing concentration of biomass-burning-based aerosol and poorer local and regional air quality through the short- and long-range transport of wildfire smoke(Filonchyk et al., 2022). To quantify the contribution of biomass-burning-based BC to total BC, we also assess the aerosol light absorption measurement capabilities and source apportionment performance based on the standard UV-IR aethalometer source apportionment mode, as well as modifications to the aethalometer source apportionment model to improve performance (Sandradewi et al., 2008a; Healy et al., 2019; Zotter et al., 2017). Finally, we provide recommendations for selecting appropriate use cases and data post-processing methods for the MA300 micro-aethalometers.

2 Materials and Methods

2.1 Site Details and Study Period

Co-located eBC measurements with an AE33 and three MA300s were conducted at a regulatory air quality monitoring station operated by Metro Vancouver, the regional regulator, at Clark Drive, a busy road junction with six travel lanes. Clark Drive is a major truck route for goods movement and connects to a major regional port. This air quality station is <20 m from the roadway and is equipped with several reference-grade instruments, including the AE33, to monitor near-road pollutant concentrations (Healy et al., 2019; Wang et al., 2018). The MA300s were co-located at the Clark Drive station for 14 weeks (August 15 to November 30, 2020). During this period, the Greater Vancouver Area experienced wildfire smoke originating from within the province of British Columbia and other parts of western North America (Nguyen et al., 2021), with days (n=11) exceeding 24-h average $PM_{2.5}$ concentrations of 25 $\mu g\,m^{-3}$. We divide the sampling window into two distinct periods, based on the days Metro Vancouver issued air quality advisories: September 8 through 18 as "Wildfire days" and the rest as "Regular days".

https://doi.org/10.5194/amt-2022-278
Preprint. Discussion started: 4 November 2022


Atmospheric Measurement Techniques Discussions

2.2 Aethalometers

Concentrations of eBC were measured using two different types of aethalometers, a 7-wavelength AE33 (Magee Scientific, California) and three individual 5-wavelength MA300s (AethLabs, San Francisco, California). Both aethalometers use a Dual-Spot mechanism and can measure aerosol absorption in multiple wavelengths in real-time. Details on the Dual-Spot aethalometer sampling mechanism have been provided elsewhere (Drinovec et al., 2015; Rajesh and Ramachandran, 2018). The AE33 was operated at a flow rate of 5 $\mathrm{L\,min^{-1}}$ with a time resolution of 1 min and comes embedded with a real-time non-linear correction mechanism (Drinovec et al., 2015). We installed three MA300 units (hereafter referred to as MA300A, MA300B, and MA300C) in parallel with the AE33. The MA300s were operated at a flow rate of 150 $\mathrm{mL\,min^{-1}}$ with a data collection frequency of 1 min. Data from MA300s include dual channel five wavelength raw photometer measurements along with compensated eBC (eBC_c) mass concentrations corrected by the onboard algorithm (Virkkula et al., 2007). More details on the two instruments and operational differences are provided in the Supporting Information (Table S2). All four aethalometers were connected to the same sampling line fitted with a 1 $\mu\mathrm{m}$ cyclone to eliminate any additional sampling artifacts. Since the AE33 and MA300 operate on different wavelength channels, we considered five wavelengths (370, 470, 520, 660, and 880 nm) from the AE33 as closest to the MA300's operating wavelengths (375, 470, 528, 625, 880 nm) and compared their results. For simplicity, these wavelength channels were renamed as UV (370-375 nm), Blue (470 nm), Green (520-528 nm), Red (625-660 nm) and IR (880 nm).

2.3 Dual-Spot Aethalometer Correction Algorithm

Both the AE33 and the MA300 use Dual-Spot sampling technology, where aerosols are collected on two filter spots at different flow rates, and measurement of the light attenuation is taken at multiple wavelengths through comparison with a reference (zero aerosol loading) spot. The outputs from the sample-loaded spots are then combined in order to estimate real-time eBC concentration, as aerosol loading will occur differently and any non-linearity in continuous measurement can be compensated by the dual spot results. Filter-based light absorption techniques are subject to measurement artifacts due to scattering on the filter, scattering of loaded aerosols or due to some particles being shadowed by others (Weingartner et al., 2003). Therefore, aethalometers require proper estimation of loading compensation factors and multiple scattering factors for accurate measurement (Virkkula et al., 2007; Weingartner et al., 2003; Virkkula et al., 2015).

In both the AE33 and MA300, wavelength-specific light attenuation (ATN) is measured by the three detectors (two on the loaded spot and one on the reference spot), and is obtained by equation 1.

$$ATN_1 = -ln(I_1/I_0)$$
$$ATN_2 = -ln(I_2/I_0)$$

I_0, I_1 and I_2 are photometer signals from the reference spot, loading spot 1, and loading spot 2, respectively. The AE33 utilizes the Drinovec et al. (2015) correction where ATN measurements (0-120) at each time stamp are converted into a compensated absorption coefficient (b_{abs}, λ) using equation 2. Finally, the eBC mass concentrations are derived by dividing the

https://doi.org/10.5194/amt-2022-278
Preprint. Discussion started: 4 November 2022


Atmospheric Measurement Techniques Discussions

IR channels' absorption coefficients by the corresponding mass absorption cross-section (MAC, σ_{air} in $\mathrm{m^2\,g^{-1}}$) as provided by the manufacturer (equation 3).

$$b_{abs}(\lambda) = \frac{A.\Delta ATN_1(\lambda)}{F_1.(1-\xi).C.(1-k.ATN_1(\lambda)).\Delta t.100} \tag{2}$$

$$eBC = \frac{b_{abs,880}}{\sigma_{air,880}} \tag{3}$$

In equation 3, k and C refer to the loading and multiple scattering correction factors, respectively. A detailed description of the notation has been provided in the Supporting Information (Section A). The scattering correction factor (C) depends on the type of filter material (Drinovec et al., 2015; Bernardoni et al., 2021; Drinovec et al., 2017); for the AE33, we use a value of 1.39 for the TFE coated glass fiber filter (M8060). The recommended filter lateral leakage factor (ξ) was set to 0.01, representing 1% leakage of the tape. The wavelength-specific loading correction factor (k) is calculated by solving a non-linear equation consisting of flow (F) and attenuation measurements (ATN) at each time step from both channels (equation 4).

$$\frac{F_2}{F_1} = \frac{ln(1-k.ATN_2)}{ln(1-k.ATN_1)} \tag{4}$$

In contrast, MA300's onboard algorithm uses a linear loading correction scheme Virkkula et al. (2007) for the operational ATN range (0-100) at each time stamp and assumes a scattering correction factor of 1.3 (from Firmware v1.09) for the PTFE filter material. It is important to note that MA300 corrections do not include any filter leakage parameters and use higher MAC values as compared to AE33. Details on the MA300's onboard algorithm and MAC values used in this work have been provided in the Supporting Information (Section B and Table S1).

2.4 Modified Drinovec Method in MA300

To compare the effect of loading correction on MA300 measurements, we utilized the raw light absorption data from the MA300s and applied a modified version of the Drinovec et al. (2015) method. We utilized the raw photometer data from MA300s and equations 1-4 to estimate non-corrected b_{abs} ($b_{abs,NC}$), followed by calculating the loading correction factor (k) and Drinovec compensated b_{abs} ($b_{abs,D}$). We observed that the MA300 sensor data was affected by both drift and post-filter-change transient effects. The drift in the photometer data was removed by calculating statistical outliers before calculating ATN and has been explained in detail in the Supporting Information (Section C). In the Drinovec et al. (2015) correction algorithm, loading effect estimations are sensitive to flow fluctuations (equation 4) and transient effects from filter changes. By inspecting the transient effect in the MA300 data, we identified a modified ATN range (15<ATN<30) for linear fitting, which differs from the AE33 range (10<ATN<30).

https://doi.org/10.5194/amt-2022-278
Preprint. Discussion started: 4 November 2022


Atmospheric Measurement Techniques Discussions

2.5 Aerosol Light Absorption Characteristics

Aerosol light absorption coefficients (b_{abs} (λ), Mm^{-1}) are an important parameter in understanding spectral light interactions. b_{abs} evaluated from aethalometers in conjunction with additional light scattering measurements can be used to derive single scattering albedo (SSA), a parameter used in studying the radiative impact of atmospheric aerosol (Rajesh and Ramachandran, 2018). Furthermore, multi-wavelength b_{abs} data are essential for real-time source apportionment of eBC (Sandradewi et al., 2008b; Zotter et al., 2017). Although estimation of SSA and radiative properties are outside the scope of this work, we focus on evaluating the b_{abs} back-calculated from the aethalometer-reported compensated eBC concentrations in order to assess the source apportionment capabilities of the MA300. For individual wavelengths, aerosol absorption coefficients (b_{abs} (λ), Mm^{-1}) were calculated using equation 5, in which reported eBC concentrations across the 5 wavelengths are multiplied by their respective MAC_λ values. We also calculated the modified Drinovec et al. (2015)-corrected MA300 $b_{abs,D}$ values to assess any potential performance improvements.

$$b_{abs}(\lambda) = eBC_\lambda \times MAC_\lambda \tag{5}$$

Spectral light absorption coefficients ($b_{abs}(\lambda)$) exhibit a power law relationship (equation 6) (Kirchstetter et al., 2004; Moosmüller et al., 2011). The power law exponent (α), i.e., the Absorption Ångström exponent, is a quantity that is used to measure the spectral dependence of light absorption and has been used as a metric to understand the source of absorbing aerosols. Higher values of α (>1), imply a higher spectral dependence of light absorption by the sample (Garg et al., 2016). A pure BC aerosol particle is a strong absorber over the whole spectrum (near-UV to near-IR); hence it shows a weak spectral dependence ($\alpha_{BC} = 1$).

$$b_{abs} \approx \lambda^{-\alpha} \tag{6}$$

From a 5 or 7-wavelength aethalometer, α can be derived from a log-linear regression between b_{abs} and wavelength (λ) on a log-log scale (Stampfer et al., 2020). However, the use of a wavelength pair (λ_1, λ_2) for the determination of α is more common and has been utilized in several source-apportionment-based studies (Segura et al., 2014; Zotter et al., 2017). In this work, we estimated α values using the multi-wavelength power law fit of b_{abs} values.

2.6 Source Apportionment using Aethalometer Data

Identification of the source of eBC particles was performed using the "Aethalometer model" (Sandradewi et al., 2008a). This method is based on assuming two different source components of eBC (fossil fuel eBC, or eBC_{ff} and biomass burning eBC, or eBC_{bb}) (Sandradewi et al., 2008a; Healy et al., 2017; Rajesh and Ramachandran, 2017; Deng et al., 2020). Sources for biomass-burning eBC include wood burning, wildfire smoke, and solid fuel burning, and fossil fuel eBC includes vehicle/traffic emissions. The two-component model strongly depends on the constrained values of α_{ff} and α_{bb} which have been reported

https://doi.org/10.5194/amt-2022-278
Preprint. Discussion started: 4 November 2022


Atmospheric Measurement Techniques Discussions

for different combinations of wavelengths elsewhere (Zotter et al., 2017). Equations for the source apportionment (SA) can be found in Supplementary Information (Section D). In this study, we performed SA for the two pairs of wavelengths using the constrained α_{ff} and α_{bb} values from Zotter et al. (2017):

1. UV-IR with α pairs as 0.9 (α_{ff}) and 2.09 (α_{bb})
2. Blue-IR with α pairs as 0.9 (α_{ff}) and 1.75 (α_{bb})

To further assess the performance of different artifact correction protocols, SA calculations were performed separately on three sets of b_{abs} values from the AE33 and MA300s:

1. b_{abs} from AE33: Instrument reported data used as reference measurement
2. b_{abs} from MA300: Instrument reported data with onboard correction
3. $b_{abs,D}$ from MA300: Drinovec corrected data from MA300's raw measurement

Apportioned components of b_{abs} ($b_{abs,bb}$ and $b_{abs,ff}$) were converted to eBC_{bb} and eBC_{ff} using equation 5. Assuming constant MAC (Table S1) values may lead to uncertainty in estimation (Segura et al., 2014; Wang et al., 2021; Zotter et al., 2017; Garg et al., 2016) as aerosol originated from biomass burning likely has different composition and light absorption characteristics than that of fossil-fuel-derived aerosol.

2.7 Data Analysis

Data collected from the aethalometers were temporally aggregated to avoid any additional sampling noise (Hagler et al., 2011). We chose the hourly average to remain consistent with previous studies used in a similar context. For QA/QC of the AE33 data, we removed any flagged data points (filter spot change, internal tests) as a part of post-processing the data. Similar flagged data points were eliminated from MA300 units from the raw data files. During the measurement period, we also identified unusually elevated concentrations of $PM_{2.5}$ for three days (October 31 - November 2, 2020) during the "Regular" period, which was attributed to local fireworks from Halloween celebrations. These three days of data were removed from the analysis to increase the consistency of the data.

The performance of the MA300 was assessed for both precision (via unit-to-unit variability) and accuracy (via linear regression against the AE33). Accuracy assessment metrics included slope, R^2, and $bR2$ (multiplication of slope and R^2). Additionally, mean absolute error (MAE), root mean square error (RMSE), and normalized root mean squared error (NRMSE) were calculated. More details about these metrics and methods have been explained in detail in the Supporting Information (Section E). All the statistical analysis, error calculations and instrumental analysis were performed in R (version 4.0.3), with a suite of open-source packages (TidyVerse (Wickham et al., 2019), OpenAir (Carslaw and Ropkins, 2012), hydroGOF (Zambrano-Bigiarini, 2020)).

https://doi.org/10.5194/amt-2022-278
Preprint. Discussion started: 4 November 2022


Atmospheric Measurement Techniques Discussions

3 Results and Discussion

Data collected from AE33 and the MA300s (A, B, and C) during the campaign were separated into wildfire-affected days (WF) and regular days (Reg). At first, we compare the instrument-reported eBC concentration from MA300 and AE33. It is important to note that aethalometer-reported eBC concentrations are derived from IR channel absorption only. Next, we explore the effect of loading correction on the MA300's raw data by applying a modified version of the Drinovec et al. (2015) method. Finally, we investigate the performance of the paired-wavelength Aethalometer Model on source identification of eBC using MA300 data.

3.1 eBC mass concentration during the study period

An hourly statistical summary of eBC mass concentration for Reg and WF period from the four aethalometers is presented in Table 1. Reference Aethalometer AE33 reported eBC concentration ranged between 0.015–10.85 $\mu g\,m^{-3}$, with a periodical average of 1.3 $\mu g\,m^{-3}$ during Reg and 4.4 $\mu g\,m^{-3}$ during WF. The average within-day hourly eBC concentration during the Reg period varied from 0.75 to 2.06 $\mu g\,m^{-3}$, with the lowest observed concentrations from 1:00 AM to 4:00 AM and the highest observed concentration from 6:00 AM to 10:00 AM. This diurnal concentration profile follows the traffic count of the junction, indicating the influence of significant sources as the vehicular emissions, which is consistent with previous near-road studies (Healy et al., 2017, 2019). However, the effect of wildfire smoke raised the concentration range of diurnal variation of eBC, with the lowest reported value of 3.1 $\mu g\,m^{-3}$ to the highest of 6.1 $\mu g\,m^{-3}$ during the WF period. The observed effect in eBC concentration due to wildfire smoke compared to the Reg period was consistent with previously studied wildfire episodes in similar regions (Healy et al., 2019). Time-series of aethalometer reported eBC concentration during the WF period has been provided in Supplementary Information (Figure S2)

3.1.1 Comparison of MA300 vs. AE33 reported eBC

The average eBC concentration reported by the three MA300 units was lower by 8% during the Reg period and 9% during the WF period than the AE33 measurements. In a previous study, Blanco-Donado et al. (2022) identified an average difference of 9% in the MA200 (sister model of MA300) reported eBC concentration and AE33 reported eBC concentration. Diurnal variation of hourly eBC reported by MA300 units ranged between 0.72 to 1.9 $\mu g\,m^{-3}$ during Reg and 2.9 to 5.2 $\mu g\,m^{-3}$ during WF period, consistently lower than the AE33's reported values. In Figure 1(a), we present the scatter plot of the MA300 reported hourly eBC concentration against the AE33 reported values during the campaign. From the linear fit in the scatter plots, we estimated an R^2 = 0.9 when MA300s were compared against AE33's data. Estimated R^2 values from MA300's data in this study were found to be consistent with previous studies (Kuula et al., 2020; Alas et al., 2020) with similar MA-series sister aethalometer models (MA200, MA350). Mean and standard deviation of eBC measurements by the MA300 units and the AE33 have been presented in the Table:1, separated by Reg and WF periods. In Reg period, the estimated coefficients of variation were 80% from MA300's measurement and 79% for AE33's measurement, which reduces to 45% during WF period for both MA300 and AE33. Our results reveal that the variability of hourly eBC concentration captured by the MA300 (average

https://doi.org/10.5194/amt-2022-278
Preprint. Discussion started: 4 November 2022

Atmospheric Measurement Techniques Discussions

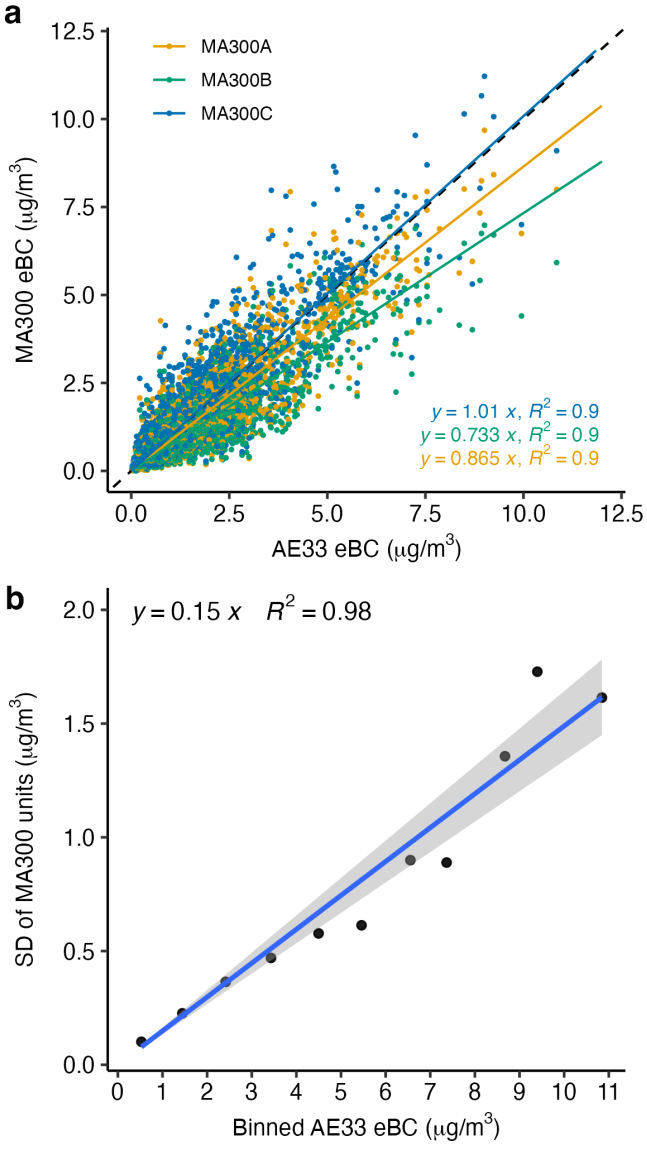

Figure 1. (a) Scatter plot of eBC mass concentration for individual MA300 units A,B and C vs AE33. The dashed line represents the 1:1 line and solid colors are the regression fit lines for the individual MA300 units; (b) Linear relationship of Standard Deviation (SD) across the three MA300 units for each bin of AE33's measurement. The blue line represents the linear fit line and the slope of the fit line represents the unit-to-unit variability.

https://doi.org/10.5194/amt-2022-278
Preprint. Discussion started: 4 November 2022


Atmospheric Measurement Techniques Discussions

of three MA300 units) were similar to the AE33's measurement. The average MAE of eBC was found to be significantly higher in WF period (0.98 $\mu g\,m^{-3}$) as compared to Reg period (0.44 $\mu g\,m^{-3}$) (Table S3(a)). Increased absolute error in WF period can be attributed to the higher observed concentration of eBC. However, the estimated (Table S3(a)) normalized error (NRMSE) was comparatively higher in Reg period (47%) than WF period (29%). Increased NRMSE in the Reg period can be explained by the uncertainty in the measurement in true lower concentrations as the range of measurement and limit of detection for a particular temporal averaging period will differ by instrument type; in addition, the presence of extreme data ranges during the WF period might normalize the errors in MA300 data.

3.1.2 Unit-to-unit variability of MA300 reported eBC

The linear fit results in Figure 1(a) indicate that AE33 reported eBC concentration were well captured by the MA300 units during the whole campaign. However, we observed variability in the slope of the linear fit line across the MA300 units (0.73–1.01), highlighting the presence of unit-to-unit variability. The range of slopes estimated from this study is consistent with other reported slopes from MA-series instruments when compared against a reference monitor (Kuula et al., 2020; Alas et al., 2020; Blanco-Donado et al., 2022). To assess the unit-to-unit variability of MA300s, we adapt the methodology from Müller et al. (2011a), where instruments of the same make and type were evaluated against a reference instrument. The ratio of the standard deviation across MA300 units and the reference instrument is representative of the coefficient of variability against the reference measurement. For each one $\mu g\,m^{-3}$ bin of AE33's measurements, mean observed concentrations for individual MA300 units were derived. We then fit the standard deviation across MA300 unit mean concentrations with the AE33's binned concentration, presented in Figure 1(b). The slope of this linear fit line has been calculated as 0.15, indicating a 15% variability across MA300 units of hourly eBC mass concentration. This variability increases to 21% when a pooled standard deviation across MA300 units (i.e., all MA300 measurements) for each bin of AE33's measurement was adopted (Figure S8). The variability in the multiple units of similar instruments can be partially explained by the instrumental measurement noise (Müller et al., 2011a). Typically, the aethalometer's instrumental noise is defined as the single standard deviation of the eBC mass concentration with particle-free air (Müller et al., 2011a; Cuesta-Mosquera et al., 2021), which has been reported as 0.032 $\mu g\,m^{-3}$ for AE33 (Cuesta-Mosquera et al., 2021). Due to the absence of particle-free measurements in our study, we assume 0.032 $\mu g\,m^{-3}$ as our reference noise levels. The noise estimates in MA-series aethalometers can be much higher (1.5 to 5 times) than the reference instrument and depend on the averaging period (Holder et al., 2018). This noise can be attributed to the strong impacts from the filter loading correction, as MA-series aethalometers were previously found to be impacted by pronounced filter-loading effect at high eBC concentration when compared to AE33 (Alas et al., 2020).

3.2 Multi-wavelength b_{abs}

Absorption coefficients, b_{abs} were derived for the five wavelengths (also referred to as channels) from the aethalometer reported multi-wavelength mass concentrations.

https://doi.org/10.5194/amt-2022-278
Preprint. Discussion started: 4 November 2022

Atmospheric Measurement Techniques Discussions

Table 1. Statistical summary (Mean and standard deviation) of eBC, and multi-wavelength b_{abs} from the four aethalometers used in this study. Summaries were calculated for the two periods (Reg and WF) separately.

Parameter	Device	**Reg (n=2082)**		**WF (n=238)**	
		Mean	**SD**	**Mean**	**SD**
eBC ($\mu g/m^3$)	AE33	1.33	1.05	4.38	2.00
	MA300A	1.18	0.98	4.05	1.79
	MA300B	1.03	0.83	3.36	1.52
	MA300C	1.44	1.17	4.50	2.02
$b_{abs,UV}(Mm^{-1})$	AE33	29.29	23.97	151.66	82.15
	MA300A	31.53	26.13	145.10	80.39
	MA300B	26.67	22.20	123.52	72.59
	MA300C	38.64	31.58	146.99	78.65
$b_{abs,Blue}(Mm^{-1})$	AE33	22.46	17.64	86.81	41.21
	MA300A	24.81	20.16	96.98	46.41
	MA300B	20.70	16.92	79.10	40.26
	MA300C	30.35	24.61	103.00	47.92
$b_{abs,Green}(Mm^{-1})$	AE33	19.25	15.05	69.35	31.89
	MA300A	21.35	17.29	78.58	34.94
	MA300B	17.90	14.53	63.68	30.75
	MA300C	25.93	20.96	83.93	37.54
$b_{abs,Red}(Mm^{-1})$	AE33	14.17	11.10	48.33	21.86
	MA300A	17.46	14.15	61.82	27.58
	MA300B	14.66	11.89	49.80	23.15
	MA300C	21.10	17.07	66.57	29.22
$b_{abs,IR}(Mm^{-1})$	AE33	10.36	8.17	34.03	15.48
	MA300A	11.91	9.95	40.99	18.09
	MA300B	10.45	8.45	33.96	15.35
	MA300C	14.61	11.82	45.50	20.47

3.2.1 Multi-wavelength b_{abs} characterized by AE33

During the Reg period, AE33's average b_{abs} were calculated as 29.3, 22.5, 19.3, 14.2, and 10.4 Mm^{-1} for UV, Blue, Green, Red and IR channels, respectively. The effect of WF smoke caused increased light absorption across the spectral channels (Table 1). As mentioned in equation 6, the strength of spectral light absorption can be evaluated by fitting a power law to the

https://doi.org/10.5194/amt-2022-278
Preprint. Discussion started: 4 November 2022

Atmospheric Measurement Techniques Discussions

absorption coefficients. Wavelength dependence on the b_{abs} for the AE33 is shown in Figure.S3 for the two periods. During the WF period, $b_{abs,UV}$ increased by a factor of 5 (from 29.3 Mm^{-1} to 152 Mm^{-1}), whereas the $b_{abs,IR}$ enhancement over the Reg period was slightly lower, by a factor of 3 (from 10.4 Mm^{-1} to 34 Mm^{-1}) (Table 1). The absorption enhancement in the UV channel reflects the elevated contribution of organic compounds originating from wildfire smoke (Healy et al., 2019; Laing et al., 2020). The exponent (α = AAE) of the spectral power power law fit was shown to be higher in the WF period (α = 1.7 from AE33) compared to the Reg period (α = 1.2 from AE33), due to the strong impact of wildfires on the enhanced light absorption in lower (UV and near-UV) wavelengths (Figure.S3). This finding is consistent with previous studies which showed similar UV enhancements during wildfire smoke and wood-burning events Helin et al. (2021); Garg et al. (2016); Laing et al. (2020).

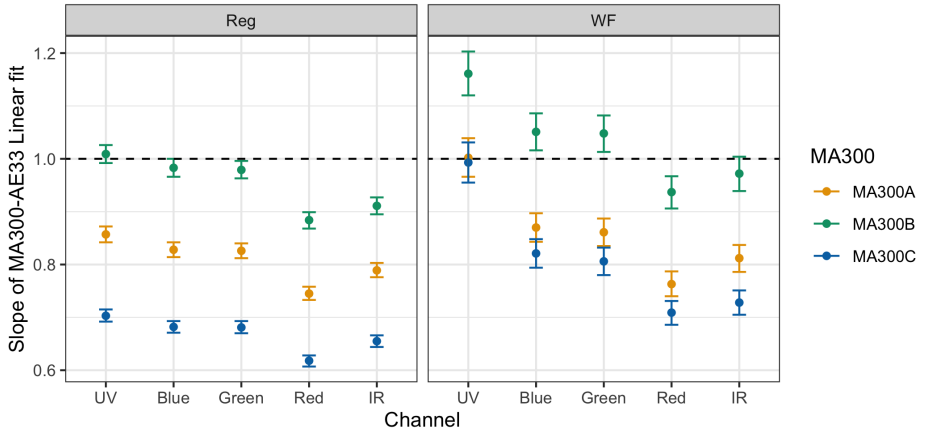

Figure 2. Slope of regression fit from the MA300's multi-wavelength b_{abs} when compared with AE33 during Reg and WF period.The dashed horizontal line is a slope of 1. The error bars show the 95% confidence interval of the linear fit for the periodical measurements.

3.2.2 Comparing MA300 b_{abs} with AE33

Statistical summary of b_{abs} from the MA300 units for the five channels were presented in Table 1. Average measurements of the three MA300 units were found to be over estimating $b_{abs,IR}$ by 18% during both the periods when compared against AE33. However, the overestimation percentage decreases to 10% for lower wavelength light absorption ($b_{abs,UV}$) during the Reg period and interestingly changes to underestimation during the WF period by 9%. The underestimation of $b_{abs,UV}$ during WF period can lead to erroneous source characterization results as UV and IR light absorption estimates are the primary inputs for the aethalometer source apportionment algorithm (Sandradewi et al., 2008b). For the $b_{abs,UV}$, the range of mean absolute error were in the range of 35.7–40.0 Mm^{-1} during WF period, which was three times the range observed during Reg period. Normalized errors were found as 59% during Reg and 34% during WF period. The lowest range of absolute error were found in the $b_{abs,IR}$ measurements (3.4–5.5 Mm^{-1} during Reg and 7.0–13.2 Mm^{-1} during WF period). Normalized errors in MA300's

https://doi.org/10.5194/amt-2022-278
Preprint. Discussion started: 4 November 2022

Atmospheric Measurement Techniques Discussions

$b_{abs,IR}$ were consistently found to be second highest after the Red channel irrespective of measurement period and MA300 units. Error-values for individual units have been provided in the Supplementary Information (Table S3(b)).

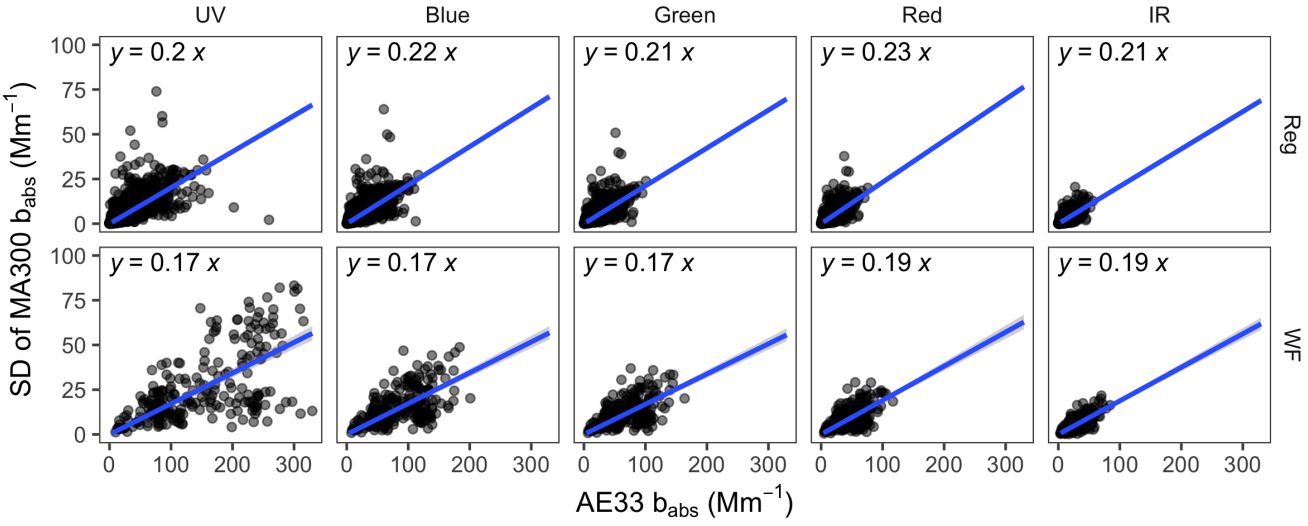

Figure 3. Standard deviation of multi-wavelength b_{abs} from the three MA300 units versus the AE33's measurements. Separate plots were generated for the different periods, top represents Reg and bottom represents WF. The blue line represents the linear fit through origin

3.2.3 Unit-to-unit variability of MA300 reported b_{abs}

Linear fit of hourly averaged b_{abs} for individual MA300 units versus AE33 revealed significant variability in the fit slopes across the spectral measurement. In Figure 2, we present the variation of spectral fit slope within individual MA300 units for the two analysis periods. During the Reg period, slopes mainly were less than 1, indicating underestimation of b_{abs} measurements. However, we observed an increased slope across the instruments during the WF period. The slope's variability in spectral measurements shows similar trends across the MA300 units, indicating the effect of instrumental sensitivity in resolving multi-wavelength b_{abs}. During the WF period, presence of increased variability can be confirmed by the increased range of 95% CI of the fit slope. In Figure 3, we identify that the unit-to-unit variability ranged 20–23% during Reg and 17–19% during WF period. Lower variability in the high pollutant period can further be explained by the errors estimated in the linear fits of MA300 vs AE33. Previously, Müller et al. (2011b), identified 9% variability of four units of aethalometer (model AE31, Magee Scientific) when compared against a reference instrument, which is lower than the case for MA300s. We find the largest spread in the standard deviation in $b_{abs,UV}$ during WF period, which can be related to large offsets in the light absorption measurements. Previously, for multi-wavelength aethalometer measurements, increased noise was identified in the near-UV wavelengths (Müller et al., 2011a).

https://doi.org/10.5194/amt-2022-278
Preprint. Discussion started: 4 November 2022

Atmospheric Measurement Techniques Discussions

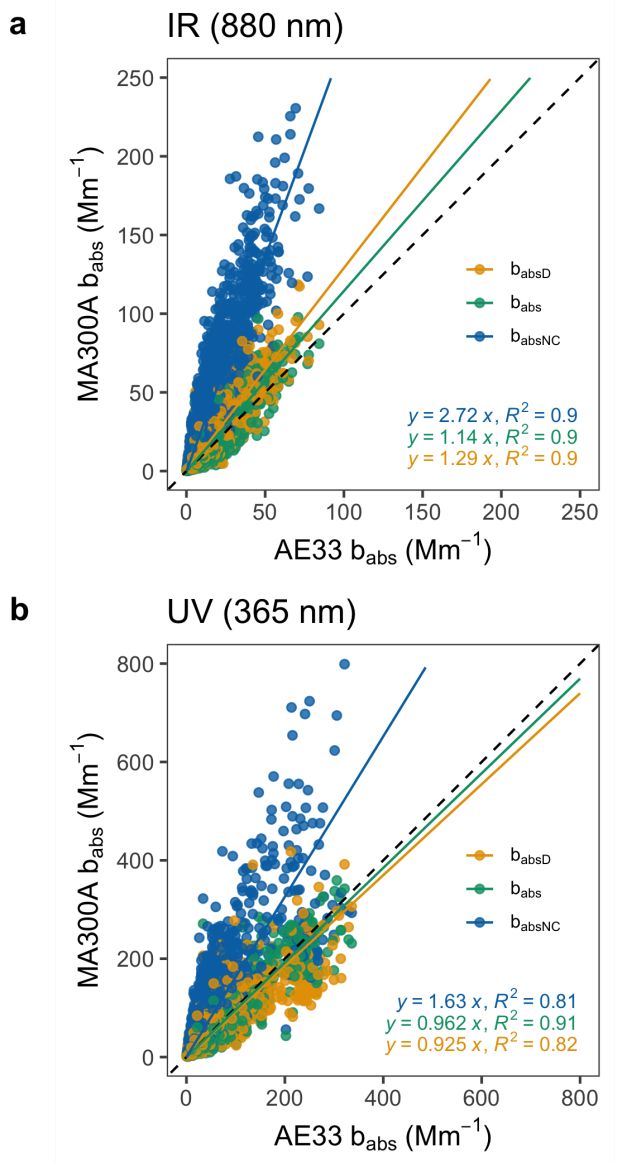

Figure 4. Scatter plot of IR (top panel) and UV (bottom panel) channel's b_{abs} from MA300A unit against the reference measurement (AE33). Dashed line represents the 1:1 line. Colors in scatter points and fit lines represent three different data set from MA300A: Data without correction (b_{absNC}), data with onboard correction (b_{abs}) and data with modified Drinovec correction(b_{absD}

https://doi.org/10.5194/amt-2022-278
Preprint. Discussion started: 4 November 2022


Atmospheric Measurement Techniques Discussions

3.3 Analysis of Loading Correction in MA300

In this section, we examine the effect of loading correction on the MA300's data for two extreme spectral measurement channels, UV and IR. In Figure 4, we compared AE33's measurement to MA300A's raw data (i.e. without correction, b_{absNC}), MA300A's onboard corrected data (i.e. with Virkkula et al. (2007) correction, b_{abs}), MA300A's modified Drinovec corrected data (i.e. with modified Drinovec et al. (2015) correction, b_{absD}). As shown in Figure 4, the onboard correction in MA300A yields an improved slope in the fit line (i.e. closer to 1) for both channels. The slope changes from 2.72 to 1.14 in IR channel and 1.63 to 0.962 in UV channel when MA300A's onboard correction adopted. Similar results were observed in the other MA300 units indicating the effectiveness of the correction scheme. Adopting the modified Drinovec correction scheme yields improvements in the fit slope (1.29 in IR and 0.93 in UV); however, the modified Drinovec correction was found to also cause additional noise in the data over the whole spectra (Table S3(c)), making it unsuitable for application in the MA300. The modified Drinovec algorithm is a non-linear algorithm (Drinovec et al., 2015) which involves flow estimates from the dual-spot aethalometer. In the case of the MA300, the air flow was found to be fluctuating in the range of -4% to 10%, which contributes to the noise in the loading-correction estimates.

3.4 Source Apportionment Results

To examine the source apportionment (SA) capabilities of the MA300, we applied the widely used two-component Aethalometer Model (Sandradewi et al., 2008a) on calculated b_{abs} values and compared the results to the apportioned results from the AE33. Previously, in Section 3.3, we identify that the UV channel absorption measurements, $b_{abs,UV}$, are subject to higher error than measurements at higher wavelengths. In aethalometers with multi-wavelength measurement capacity, $b_{abs,UV}$ reports highest amount of light absorption measurements in characterizing ambient aerosols, which essentially drives the filter movement due to the fastest ATN increase(Drinovec et al., 2015). Although the MA300's $b_{abs,UV}$ showed a better linear relationship with AE33 during the WF period, it was subjected to more noise. It was previously identified that PTFE filter based micro-aethalometers were susceptible to deviations in light absorption measurements irrespective of a clean or aerosol loaded filter spot(Düsing et al., 2019). In our study, MA300s were subjected to strong loading effect in addition to RH changes during the sampling. Further, wildfire smoke affected aerosols can become hygroscopic with aging as compared to freshly emitted soot particles from diesel vehicle emission. Hence, the combined effect of imposed noise due to filter loading correction, and highly loaded hygroscopic aerosol can interact with water vapor and filter materials, which can significantly impact the UV-channel light absorption measurements. Given these challenges, UV and IR channel based SA results might not be suitable in cases where the instrument's noise exceeds the true spatio-temporal differences. As an alternative, the Blue-IR channel pairing can also be adopted for source apportionment (Zotter et al., 2017; Deng et al., 2020) and MA300 photometer measurements from the Blue channel were more accurate and precise as compared to the UV channel. To assess source apportionment performance at distinguishing biomass burning (BB) and fossil fuel (FF) derived eBC, we use b_{abs} data from both artifact correction mechanisms (MA300 onboard and modified Drinovec) and two wavelength pairs (UV-IR and Blue-IR).

https://doi.org/10.5194/amt-2022-278
Preprint. Discussion started: 4 November 2022

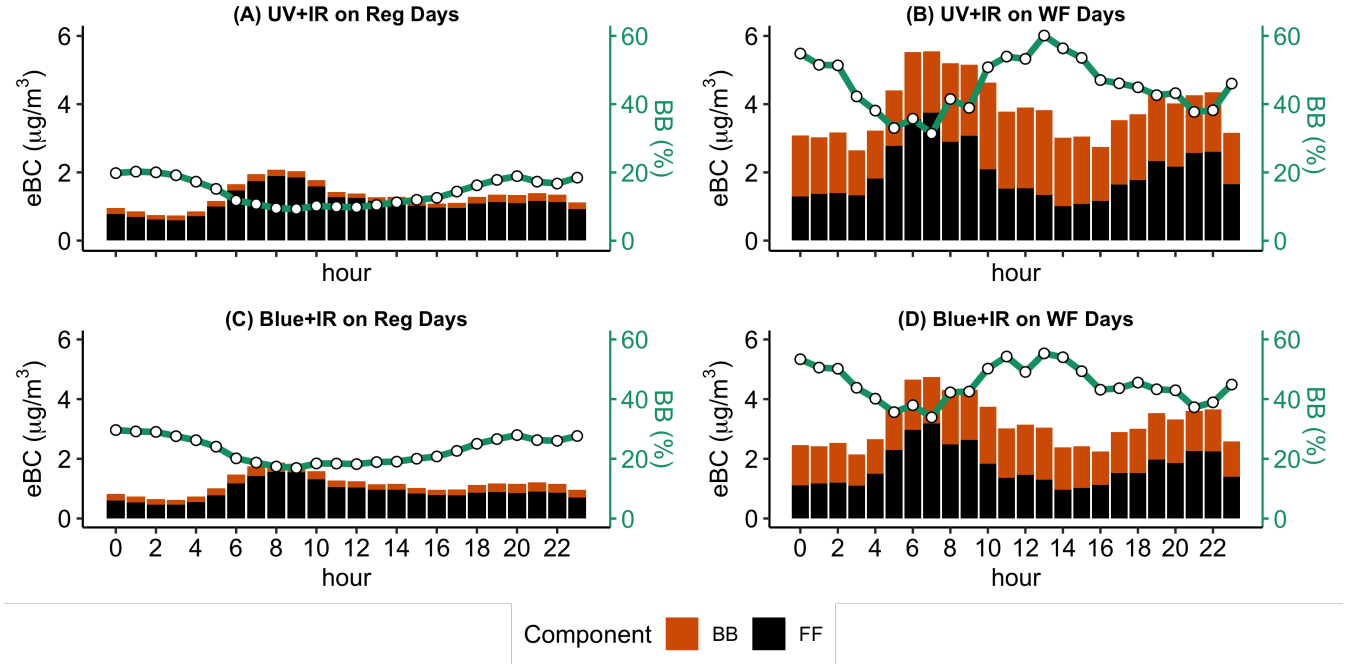

Figure 5. Diurnal variation of AE33 reported eBC contribution from BB and FF sources during regular (Reg) days and wildfire smoke affected (WF) days. Panels A-B are for the UV-IR pairs, Panels C-D are for the Blue-IR pairs. Wildfire smoke affected days are in Panels B and D and Regular days are in panels A and C. The green line (right axis) represents the percentage of eBC mass from biomass burning during the measurement period.

3.4.1 Source Apportionment Results from AE33

Figure 5 shows the diurnal variation of AE33 reported eBC concentration and its contribution from eBC_{bb}, eBC_{ff}, and percentage contribution of eBC_{bb} to the total eBC (BB(%)) during the measurement period using both the UV-IR and Blue-IR method. The diurnal variation of eBC components is consistent with patterns observed in previous studies (Rajesh and Ramachandran, 2017; Healy et al., 2019; Deng et al., 2020), with increased concentration of eBC_{ff} during the morning and evening hours coinciding with peak traffic flows, and likely contributions from fresh diesel emissions. Using the UV-IR based SA method (Panel A and B from Figure 5), daily eBC_{ff} concentrations were in the range of 0.6 – 1.9 $\mu g\,m^{-3}$ during Reg period and in 1.0 – 3.8 $\mu g\,m^{-3}$ during WF period. eBC_{bb} concentrations were found to be in the range of 0.1 – 0.2 $\mu g\,m^{-3}$ during Reg period and 1.3 – 2.6 $\mu g\,m^{-3}$ during WF period. The calculated percentage contribution of eBC_{bb} to total eBC emissions (BB%) was 9 – 20% during the Reg period and 31 – 60% during the WF period. Even though the traffic emissions dominated the location of aerosol sampling, the biomass burning contributions in REG period, have been previously hypothesized to originate from local household wood burning sources (Healy et al., 2019) with the highest concentrations during the evening to late night. During the WF period, the enhanced eBC concentration was majorly contributed by the biomass burning components, eBC_{bb}; however, we hypothesize that the enhancement of eBC_{ff} may be due to two major factors. Firstly, there may have been a real

https://doi.org/10.5194/amt-2022-278
Preprint. Discussion started: 4 November 2022


Atmospheric Measurement Techniques Discussions

increase in the number of heavy-duty vehicles during the early morning and evening hours that coincided with the WF period, increasing the eBC emission from fossil fuel-based sources. Secondly, during wildfire smoke-affected days, aerosols can be a complex mixture of fresh and highly aged components and using a fixed pair of α for the source apportionment model may not accurately separate eBC in two components (Garg et al., 2016). Hence, the contribution of eBC_{ff} during the WF period increases as the overall eBC increases, even if the BC is estimated from a highly mixed environment. Blue-IR based results (Panel C and D from Figure 5) show that eBC_{ff} mass concentration tend to underestimate by 16% on average (20% during Reg and 14% during WF period) as compared to UV-IR results. In the case of biomass burning-based source contribution, eBC_{bb}, 22% underestimation was identified during the WF period using Blue-IR based SA instead of UV-IR. Utilizing Blue-IR method based source apportionment resulted, 41% overestimation of eBC_{bb} component, however the absolute component concentration was measured as lowest of all the components (Figure S5). We believe, this overestimation can be a statistical artifact, arising from weak biomass burning signal during Reg period. As identified in Zotter et al. (2017), SA results can have additional uncertainties when different wavelength pairs are chosen. Hence using Blue-IR based SA in Reg days may not appropriately separate the biomass burning based eBC component due to the weak light absorption signal from the Blue channel. These results indicate that using Blue-IR based SA can influence the estimated absolute mass concentrations of eBC_{bb}; however, the diurnal variation of the relative contribution of BB% remains fairly similar to UV-IR based SA results.

3.4.2 Source Apportionment Results from MA300

The diurnal profiles of the apportioned components of MA300 eBC (average of the three units) were calculated and are provided in the supporting information (Figure S6 and S7). For each SA technique (Wavelength pairings: UV-IR or Blue-IR) and correction methods applied (MA300's Onboard or Drinovec), we also calculated the percentage difference between the results from MA300 and AE33 eBC_{bb}, eBC_{ff} and BB(%) values, for the two periods (Reg and WF), presented in Figure 6. From the diurnal patterns of MA300's SA results (Figure S10), we identify that the UV-IR based eBC_{ff} mass concentrations were in the range of 0.7 – 1.7 $\mu g\,m^{-3}$ and 1.8 – 3.9 $\mu g\,m^{-3}$ during Reg and WF period respectively. This range changes to 0.6 – 1.5 $\mu g\,m^{-3}$ and 1.5 – 3.3 $\mu g\,m^{-3}$ for Reg and WF period respectively when Blue-IR SA method applied. For eBC_{bb}, the concentration ranges were 0.1 – 0.16 $\mu g\,m^{-3}$ during Reg period, 0.8 – 1.7 $\mu g\,m^{-3}$ during WF period for UV-IR based SA and 0.1 – 0.2 $\mu g\,m^{-3}$ during Reg period, 0.7 – 1.4 $\mu g\,m^{-3}$ during WF period for Blue-IR based SA. Adapting Blue-IR wavelength pair on MA300 had similar effect on under/over estimation of eBC components as observed for AE33 (Figure S5), suggesting that the influence of wavelength pair selection is consistent across instrument types. In Table S5, we summarized the estimated diurnal mean and standard deviation of different SA results from the instruments. From Figure 6, we find that the MA300 eBC components were mostly underestimated as compared to AE33's apportioned concentration. In Reg period, MA300 reported eBC_{bb} was underestimated by up to 50% to the AE33's data. However, the difference in eBC_{ff} was found to become occasionally positive and were within $\pm$40%. Late night periods with low traffic conditions (i.e. fewer eBC_{ff} sources) may present challenges for MA300 data collection, and contribute to overestimation of eBC_{ff}. The benefits of using Blue-IR based SA method on MA300's are most evident during the WF period. By adopting Blue-IR based SA instead of UV-IR wavelength, we find improved (lowering difference in MA300 to AE33) source characterization results by MA300s.

https://doi.org/10.5194/amt-2022-278
Preprint. Discussion started: 4 November 2022

Atmospheric Measurement Techniques Discussions

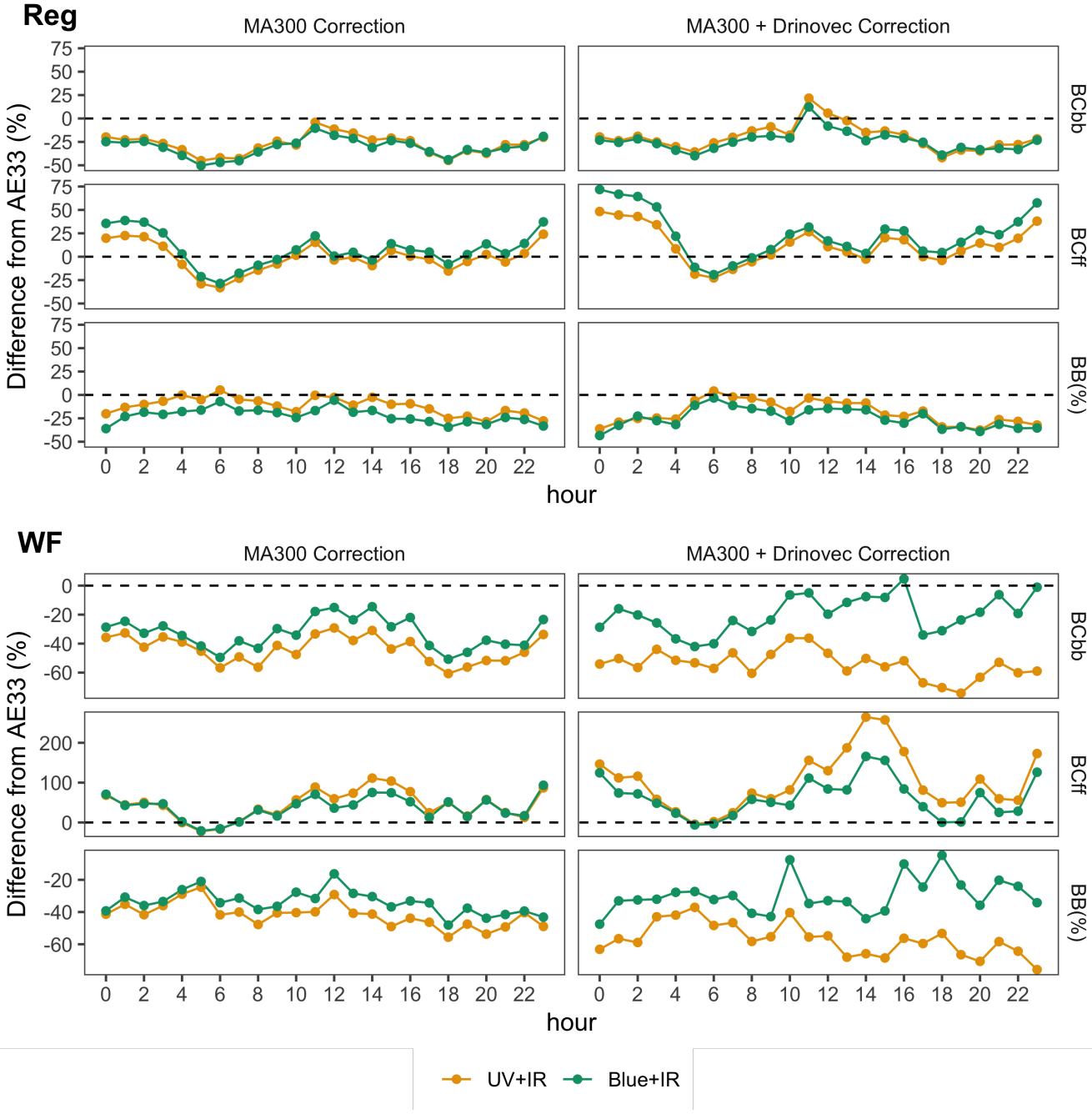

Figure 6. Percentage difference of hourly SA results in between MA300 and AE33. Average MA300's onboard corrected data and Drinovec-corrected MA300 are data treated separately for the two periods (Reg and WF). SA results from UV+IR and Blue+IR wavelength pair have been evaluated separately

https://doi.org/10.5194/amt-2022-278
Preprint. Discussion started: 4 November 2022


Atmospheric Measurement Techniques Discussions

The percentage difference reduces from -44% to -33%, 44% to 37%, and -42% to -34% for eBC_{bb} concentration, eBC_{ff} concentration, and BB(%) respectively. We see similar improvement in the Drinovec corrected MA300s data, however, as previously noted, the concentration profile for Drinovec corrected MA300 data is susceptible to noise. Figure 6 also shows how the percentage difference between MA300 and AE33 source characterization varies diurnally. Highest differences in the eBC_{ff} were observed during low traffic periods, which are likely to have increased uncertainty as b_{abs} measurements might fall beyond the detection limit (Backman et al., 2017). From the Drinovec corrected SA results, we find the that the diurnal range percentage difference (Figure 6) in eBC components were higher during the WF period. This observation aligns with the previously estimated increased errors in Drinovec corrected data, offsetting the SA results from AE33. The impact of additional noise in MA300's SA results by Drinovec correction can also be visible in hours with low concentration, particularly during the Reg period. However, the Blue-IR based SA on Drinovec corrected data reduces the percentage difference of MA300's eBC components from AE33.

4 Summary and Conclusions

In this we study, we have characterized the performance of the MA300 micro-aethalometer against the AE33 aethalometer, identifying potential strengths and limitations given different monitoring needs and user focus. We find that multi-wavelength micro-aethalometers can be used in several contexts. With the growing number of studies using MA-series micro-aethalometers (MA200, MA300 and MA350), we try to assess MA300's capability in estimating eBC concentration in real-world environments, MA300's unit-to-unit variability in assessing eBC concentrations as well as multi-wavelength absorption coefficients and MA300's source apportionment capabilities.

Overall, we found that MA300s were able to reproduce the trends in eBC concentration in both Reg and WF periods, as compared to the reference-grade AE33. However, we identify that the MA300 reported concentrations were underestimated by 13% when compared against reference AE33's results. The underestimation by MA300 can be attributed to measurement uncertainty arising from sensor performance, differences in wavelength fixed MAC values and differences in the onboard correction algorithms. This underestimation could be addressed by applying post-analysis correction/calibration. The range of observed concentrations and unit-to-unit variation are also important factors to take into account in the design of a sampling strategy. In the study region, on good air quality days, observed concentrations can be lower the than the instrument's LOD (Backman et al., 2017). As the MA300 is a low flow instrument while the AE33 is a high flow one, the MA300 is less sensitive to minor temporal changes in eBC concentration. This can lead to increased measurement error in comparatively cleaner environments. However, we find that MAE of eBC measurement from MA300 (compared to the AE33) can be in the range of 0.44 – 0.98 $\mu g\,m^{-3}$ depending upon the measurement period. We observe larger MAE during high pollution conditions (e.g., WF period in this study). Based on these findings, caution may be required when MA300s are used to capture spatial or temporal differences in eBC below the 0.98 $\mu g\,m^{-3}$ threshold. In this study, we calculated hourly concentration of eBC by time integrating the instrument's data collection frequency of 5-minute and found that the hourly averaged eBC concentrations from individual MA300 units were well correlated with the reference measurements. In future applications of the MA300,

https://doi.org/10.5194/amt-2022-278
Preprint. Discussion started: 4 November 2022


Atmospheric Measurement Techniques Discussions

trade-offs between high temporal resolution and increased noise should be considered (Liu et al., 2021; Hagler et al., 2011), recognizing that temporal integration can alleviate the unit specific measurement noise. From the MA300's raw photometer readings, we identified presence of instrumental drift across the units. We were able to eliminate the drifted signals through post-processing the raw data using statistical outlier detection method. The presence of drift determines the quality of light absorption measurement and instrument's onboard algorithm does not eliminate such drifted signals, which can be due to the physical operation of the instrument, such as filter tape change (Drinovec et al., 2015) or due to environmental factors (Düsing et al., 2019).

We explored application of the latest non-linear aethalometer loading correction protocols in the MA300 by adopting a modified Drinovec correction method, but found increased noise in MA300 b_{abs} estimates across the spectra as a result. In dual-spot aethalometers, loading correction algorithms can be made robust and scientifically accurate by considering the transient effect of filter change, filter specific scattering correction parameter, flow leakage, measurement discontinuity due to filter change, which has been thoroughly considered in the algorithm proposed by Drinovec et al. (2015) and developed for model AE33. We applied a modified version of Drinovec's algorithm to MA300 raw data, and identified obstacles to its effective adoption in this instrument: we hypothesize that an inconsistency is flow fluctuation in MA300, which is a key variable in deriving the real-time loading correction parameter.

Characterizing unit-to-unit variability can speak to instrument precision, and may be particularly important for use cases where multiple MA300s are simultaneously deployed to measure a pollution event. We reported the precision of MA300 eBC in terms of unit-to-unit variability as 15%. This value is higher than that reported in the previously studied other aethalometer models: 4.3% for AE31 (Müller et al., 2011a), 0.5% for AE33 (Cuesta-Mosquera et al., 2021). For the multi-wavelength b_{abs}, the unit-to-unit variability did not show any trend along the spectral light absorption measurements. Yet, large instrumental noise was visible in the b_{absUV} measurements, which is consistent with previous studies on multi-wavelength aethalometers (Cuesta-Mosquera et al., 2021; Müller et al., 2011a).

From the five wavelength light absorption measurements, we found that the UV channel experienced the highest amount of measurement error (average MAE of 37 Mm^{-1} during WF period). Light absorption measurements in the UV channel can also be sensitive to interference from the volatile organic compounds on the filter tape Vecchi et al. (2014) or from the other light absorbing non BC combustion particles which affect lower wavelengths more than higher ones. Hence, using UV and IR channel for eBC source apportionment may be less reliable, particularly during high pollution events. As an alternative technique we tested the Blue and IR channel based source apportionment results. The UV-IR based SA method on MA300's onboard corrected data tend to underestimate eBC_{ff} and eBC_{bb} mass concentrations, however the relative contribution estimates remain comparable during Reg period. In WF period, due to discrepancies observed in UV channel's b_{abs}, 44% underestimation of eBC_{bb} and 44% overestimation of eBC_{ff} were identified. Including Blue-IR based SA resulted better estimates of eBC_{bb} and eBC_{ff} concentrations, 10% improvement in eBC_{bb} and 7% improvement in eBC_{ff}. However, it is important to note that switching to Blue-IR from UV-IR may lead to difference in estimation of components - which can be corrected by calibration with a site specific reference grade eBC monitoring system (such as AE33). For spatial source apportionment study across a region, several micro-aethalometers (like MA300s) can be utilized for localized monitoring along with a centralized state-of-

https://doi.org/10.5194/amt-2022-278
Preprint. Discussion started: 4 November 2022

the-art reference aethalometer. This can be helpful to determine the estimated change in eBC components when the wavelength pair is changed and improve the data quality of spatio-temporal source evaluation of eBC.

Code and data availability.

The data associated with this article are available at https://borealisdata.ca/dataset.xhtml?persistentId=doi:10.5683/SP3/DRQBUY. Code can be requested via the given corresponding e-mail address.

Author contributions.

The authors MC, AG and NZ were responsible for the conceptualization of the study. Data collection, data analysis, and the methodology development were led by MC, under the supervision of NZ and AG. Any software for processing and evaluating the data was written by MC. All figures were produced by MC. The original draft of the paper was written by MC. The review and editing of the paper was done by AG and NZ.

Competing interests.

The authors declare that they have no conflict of interest.

Disclaimer. Financial Support

This research was funded by the Natural Sciences and Engineering Research Council (NSERC) of Canada through the Discovery Grant program (RGPIN-2018-04582 and RGPIN-2018-04893). MC was supported by a Science Engineering Research Board of India Overseas Doctoral Fellowship.

Acknowledgements. We would like to thank Sakshi Jain, and Melanie MacArthur, for helping with instrument setup and data acquisition troubleshooting. We acknowledge Ken Reid and Johnny Le from Metro Vancouver for helping with the Co-location campaign at the Clark Drive site. We are grateful to receive support from Air Quality and Climate Change, Metro Vancouver Regional District, Burnaby, Canada. We are thankful to Luka Drinovec for the introduction to the AE33's compensation algorithm. We would also like to express our sincere thanks to Steven Rogak for his valuable support in conducting the preliminary laboratory experiment.

https://doi.org/10.5194/amt-2022-278
Preprint. Discussion started: 4 November 2022

Atmospheric Measurement Techniques Discussions

References

Alas, H. D. C., Müller, T., Weinhold, K., Pfeifer, S., Glojek, K., Gregorič, A., Močnik, G., Drinovec, L., Costabile, F., Ristorini, M., and Wiedensohler, A.: Performance of microAethalometers: Real-world Field Intercomparisons from Multiple Mobile Measurement Campaigns in Different Atmospheric Environments, Aerosol and Air Quality Research, 20, 2640–2653, https://doi.org/10.4209/aaqr.2020.03.0113, publisher: Taiwan Association for Aerosol Research, 2020.

Apte, J. S., Kirchstetter, T. W., Reich, A. H., Deshpande, S. J., Kaushik, G., Chel, A., Marshall, J. D., and Nazaroff, W. W.: Concentrations of fine, ultrafine, and black carbon particles in auto-rickshaws in New Delhi, India, Atmospheric Environment, 45, 4470–4480, https://doi.org/10.1016/j.atmosenv.2011.05.028, 2011.

Aurell, J., Gullett, B., Holder, A., Kiros, F., Mitchell, W., Watts, A., and Ottmar, R.: Wildland fire emission sampling at Fishlake National Forest, Utah using an unmanned aircraft system, Atmospheric Environment, 247, 118 193, https://doi.org/10.1016/j.atmosenv.2021.118193, 2021.

Backman, J., Schmeisser, L., Virkkula, A., Ogren, J. A., Asmi, E., Starkweather, S., Sharma, S., Eleftheriadis, K., Uttal, T., Jefferson, A., Bergin, M., Makshtas, A., Tunved, P., and Fiebig, M.: On Aethalometer measurement uncertainties and an instrument correction factor for the Arctic, Atmospheric Measurement Techniques, 10, 5039–5062, https://doi.org/10.5194/amt-10-5039-2017, publisher: Copernicus GmbH, 2017.

Bauer, J. J., Yu, X.-Y., Cary, R., Laulainen, N., and Berkowitz, C.: Characterization of the Sunset Semi-Continuous Carbon Aerosol Analyzer, Journal of the Air & Waste Management Association, 59, 826–833, https://doi.org/10.3155/1047-3289.59.7.826, publisher: Taylor & Francis _eprint: https://doi.org/10.3155/1047-3289.59.7.826, 2009.

Bernardoni, V., Ferrero, L., Bolzacchini, E., Forello, A. C., Gregorič, A., Massabò, D., Močnik, G., Prati, P., Rigler, M., Santagostini, L., Soldan, F., Valentini, S., Valli, G., and Vecchi, R.: Determination of Aethalometer multiple-scattering enhancement parameters and impact on source apportionment during the winter 2017/18 EMEP/ACTRIS/COLOSSAL campaign in Milan, Atmospheric Measurement Techniques, 14, 2919–2940, https://doi.org/10.5194/amt-14-2919-2021, publisher: Copernicus GmbH, 2021.

Blanco-Donado, E. P., Schneider, I. L., Artaxo, P., Lozano-Osorio, J., Portz, L., and Oliveira, M. L. S.: Source identification and global implications of black carbon, Geoscience Frontiers, 13, 101 149, https://doi.org/10.1016/j.gsf.2021.101149, 2022.

Bond, T. C. and Bergstrom, R. W.: Light absorption by carbonaceous particles: An investigative review, Aerosol Science and Technology, 40, 27–67, https://doi.org/10.1080/02786820500421521, 2006.

Carslaw, D. C. and Ropkins, K.: openair — An R package for air quality data analysis, Environmental Modelling & Software, 27-28, 52–61, https://doi.org/10.1016/j.envsoft.2011.09.008, 2012.

Cuesta-Mosquera, A., Močnik, G., Drinovec, L., Müller, T., Pfeifer, S., Minguillón, M. C., Briel, B., Buckley, P., Dudoitis, V., Fernández-García, J., Fernández-Amado, M., Ferreira De Brito, J., Riffault, V., Flentje, H., Heffernan, E., Kalivitis, N., Kalogridis, A.-C., Keernik, H., Marmureanu, L., Luoma, K., Marinoni, A., Pikridas, M., Schauer, G., Serfozo, N., Servomaa, H., Titos, G., Yus-Díez, J., Zioła, N., and Wiedensohler, A.: Intercomparison and characterization of 23 Aethalometers under laboratory and ambient air conditions: procedures and unit-to-unit variabilities, Atmospheric Measurement Techniques, 14, 3195–3216, https://doi.org/10.5194/amt-14-3195-2021, publisher: Copernicus GmbH, 2021.

Deng, J., Guo, H., Zhang, H., Zhu, J., Wang, X., and Fu, P.: Source apportionment of black carbon aerosols from light absorption observation and source-oriented modeling: an implication in a coastal city in China, Atmospheric Chemistry and Physics, 20, 14 419–14 435, https://doi.org/10.5194/acp-20-14419-2020, 2020.

https://doi.org/10.5194/amt-2022-278
Preprint. Discussion started: 4 November 2022

Drinovec, L., Močnik, G., Zotter, P., Prévôt, A. S. H., Ruckstuhl, C., Coz, E., Rupakheti, M., Sciare, J., Müller, T., Wiedensohler, A., and Hansen, A. D. A.: The "dual-spot" Aethalometer: an improved measurement of aerosol black carbon with real-time loading compensation, Atmospheric Measurement Techniques, 8, 1965–1979, https://doi.org/10.5194/amt-8-1965-2015, publisher: Copernicus GmbH, 2015.

Drinovec, L., Gregorič, A., Zotter, P., Wolf, R., Bruns, E. A., Prévôt, A. S. H., Petit, J.-E., Favez, O., Sciare, J., Arnold, I. J., Chakrabarty, R. K., Moosmüller, H., Filep, A., and Močnik, G.: The filter-loading effect by ambient aerosols in filter absorption photometers depends on the coating of the sampled particles, Atmospheric Measurement Techniques, 10, 1043–1059, https://doi.org/10.5194/amt-10-1043-2017, publisher: Copernicus GmbH, 2017.

Duc, H. N., Shingles, K., White, S., Salter, D., Chang, L. T.-C., Gunashanhar, G., Riley, M., Trieu, T., Dutt, U., Azzi, M., Beyer, K., Hynes, R., and Kirkwood, J.: Spatial-Temporal Pattern of Black Carbon (BC) Emission from Biomass Burning and Anthropogenic Sources in New South Wales and the Greater Metropolitan Region of Sydney, Australia, Atmosphere, 11, 570, https://doi.org/10.3390/atmos11060570, number: 6 Publisher: Multidisciplinary Digital Publishing Institute, 2020.

Düsing, S., Wehner, B., Müller, T., Stöcker, A., and Wiedensohler, A.: The effect of rapid relative humidity changes on fast filter-based aerosol-particle light-absorption measurements: uncertainties and correction schemes, Atmospheric Measurement Techniques, 12, 5879–5895, https://doi.org/10.5194/amt-12-5879-2019, publisher: Copernicus GmbH, 2019.

Filonchyk, M., Peterson, M. P., and Sun, D.: Deterioration of air quality associated with the 2020 US wildfires, Science of The Total Environment, 826, 154 103, https://doi.org/10.1016/j.scitotenv.2022.154103, 2022.

Garg, S., Chandra, B. P., Sinha, V., Sarda-Esteve, R., Gros, V., and Sinha, B.: Limitation of the Use of the Absorption Angstrom Exponent for Source Apportionment of Equivalent Black Carbon: a Case Study from the North West Indo-Gangetic Plain, Environmental Science & Technology, 50, 814–824, https://doi.org/10.1021/acs.est.5b03868, publisher: American Chemical Society, 2016.

Goel, V., Hazarika, N., Kumar, M., Singh, V., Thamban, N. M., and Tripathi, S. N.: Variations in Black Carbon concentration and sources during COVID-19 lockdown in Delhi, Chemosphere, 270, 129 435, https://doi.org/10.1016/j.chemosphere.2020.129435, 2021.

Gundel, L. A., Dod, R. L., Rosen, H., and Novakov, T.: The relationship between optical attenuation and black carbon concentration for ambient and source particles, Science of The Total Environment, 36, 197–202, https://doi.org/10.1016/0048-9697(84)90266-3, 1984.

Hagler, G. S., Yelverton, T. L., Vedantham, R., Hansen, A. D., and Turner, J. R.: Post-processing method to reduce noise while preserving high time resolution in aethalometer real-time black carbon data, Aerosol and Air Quality Research, 11, 539–546, https://doi.org/10.4209/aaqr.2011.05.0055, 2011.

Hansen, A. D., Rosen, H., and Novakov, T.: The aethalometer - An instrument for the real-time measurement of optical absorption by aerosol particles, Science of the Total Environment, The, 36, 191–196, https://doi.org/10.1016/0048-9697(84)90265-1, publisher: Elsevier, 1984.

Healy, R. M., Sofowote, U., Su, Y., Debosz, J., Noble, M., Jeong, C. H., Wang, J. M., Hilker, N., Evans, G. J., Doerksen, G., Jones, K., and Munoz, A.: Ambient measurements and source apportionment of fossil fuel and biomass burning black carbon in Ontario, Atmospheric Environment, 161, 34–47, https://doi.org/10.1016/j.atmosenv.2017.04.034, 2017.

Healy, R. M., Wang, J. M., Sofowote, U., Su, Y., Debosz, J., Noble, M., Munoz, A., Jeong, C.-H., Hilker, N., Evans, G. J., and Doerksen, G.: Black carbon in the Lower Fraser Valley, British Columbia: Impact of 2017 wildfires on local air quality and aerosol optical properties, Atmospheric Environment, 217, 116 976, https://doi.org/10.1016/j.atmosenv.2019.116976, 2019.

Helin, A., Niemi, J. V., Virkkula, A., Pirjola, L., Teinilä, K., Backman, J., Aurela, M., Saarikoski, S., Rönkkö, T., Asmi, E., and Timonen, H.: Characteristics and source apportionment of black carbon in the Helsinki metropolitan area, Finland, Atmospheric Environment, 190, 87–98, https://doi.org/10.1016/j.atmosenv.2018.07.022, 2018.

https://doi.org/10.5194/amt-2022-278
Preprint. Discussion started: 4 November 2022

Helin, A., Virkkula, A., Backman, J., Pirjola, L., Sippula, O., Aakko-Saksa, P., Väätäinen, S., Mylläri, F., Järvinen, A., Bloss, M., Aurela, M., Jakobi, G., Karjalainen, P., Zimmermann, R., Jokiniemi, J., Saarikoski, S., Tissari, J., Rönkkö, T., Niemi, J. V., and Timonen, H.: Variation of Absorption Ångström Exponent in Aerosols From Different Emission Sources, Journal of Geophysical Research: Atmospheres, 126, e2020JD034 094, https://doi.org/10.1029/2020JD034094, _eprint: https://agupubs.onlinelibrary.wiley.com/doi/pdf/10.1029/2020JD034094, 2021.

Holder, A., Seay, B., Brashear, A., Yelverton, T., Blair, J., and Blair, S.: Evaluation of a multi-wavelength black carbon (BC) sensor, Clean Air Soc. Australia and New ZealandLidcomeA, 2018.

Jeong, H. and Park, D.: Contribution of time-activity pattern and microenvironment to black carbon (BC) inhalation exposure and potential internal dose among elementary school children, Atmospheric Environment, 164, 270–279, https://doi.org/10.1016/j.atmosenv.2017.06.007, 2017.

Kirchstetter, T. W., Novakov, T., and Hobbs, P. V.: Evidence that the spectral dependence of light absorption by aerosols is affected by organic carbon, Journal of Geophysical Research: Atmospheres, 109, https://doi.org/10.1029/2004JD004999, _eprint: https://onlinelibrary.wiley.com/doi/pdf/10.1029/2004JD004999, 2004.

Kuula, J., Mäkelä, T., Aurela, M., Teinilä, K., Varjonen, S., González, , and Timonen, H.: Laboratory evaluation of particle-size selectivity of optical low-cost particulate matter sensors, Atmospheric Measurement Techniques, 13, 2413–2423, https://doi.org/10.5194/amt-13-2413-2020, 2020.

Lack, D. A., Moosmüller, H., McMeeking, G. R., Chakrabarty, R. K., and Baumgardner, D.: Characterizing elemental, equivalent black, and refractory black carbon aerosol particles: a review of techniques, their limitations and uncertainties, Analytical and Bioanalytical Chemistry, 406, 99–122, https://doi.org/10.1007/s00216-013-7402-3, 2014.

Laing, J. R., Jaffe, D. A., and Arthur J. Sedlacek, I. I. I.: Comparison of Filter-based Absorption Measurements of Biomass Burning Aerosol and Background Aerosol at the Mt. Bachelor Observatory, Aerosol and Air Quality Research, 20, 663–678, https://doi.org/10.4209/aaqr.2019.06.0298, publisher: Taiwan Association for Aerosol Research, 2020.

Li, X., Xiao, M., Xu, X., Zhou, J., Yang, K., Wang, Z., Zhang, W., Hopke, P. K., and Zhao, W.: Light Absorption Properties of Organic Aerosol from Wood Pyrolysis: Measurement Method Comparison and Radiative Implications, Environmental Science & Technology, 54, 7156–7164, https://doi.org/10.1021/acs.est.0c01475, publisher: American Chemical Society, 2020.

Liu, X., Hadiatullah, H., Zhang, X., Hill, L. D., White, A. H. A., Schnelle-Kreis, J., Bendl, J., Jakobi, G., Schloter-Hai, B., and Zimmermann, R.: Analysis of mobile monitoring data from the microAeth® MA200 for measuring changes in black carbon on the roadside in Augsburg, Atmospheric Measurement Techniques, 14, 5139–5151, https://doi.org/10.5194/amt-14-5139-2021, 2021.

Meena, G. S., Mukherjee, S., Buchunde, P., Safai, P. D., Singla, V., Aslam, M. Y., Sonbawne, S. M., Made, R., Anand, V., Dani, K. K., and Pandithurai, G.: Seasonal variability and source apportionment of black carbon over a rural high-altitude and an urban site in western India, Atmospheric Pollution Research, 12, 32–45, https://doi.org/10.1016/j.apr.2020.10.006, 2021.

Moosmüller, H., Chakrabarty, R. K., Ehlers, K. M., and Arnott, W. P.: Absorption Ångström coefficient, brown carbon, and aerosols: basic concepts, bulk matter, and spherical particles, Atmospheric Chemistry and Physics, 11, 1217–1225, https://doi.org/10.5194/acp-11-1217-2011, publisher: Copernicus GmbH, 2011.

Müller, T., Henzing, J. S., de Leeuw, G., Wiedensohler, A., Alastuey, A., Angelov, H., Bizjak, M., Collaud Coen, M., Engström, J. E., Gruening, C., Hillamo, R., Hoffer, A., Imre, K., Ivanow, P., Jennings, G., Sun, J. Y., Kalivitis, N., Karlsson, H., Komppula, M., Laj, P., Li, S.-M., Lunder, C., Marinoni, A., Martins dos Santos, S., Moerman, M., Nowak, A., Ogren, J. A., Petzold, A., Pichon, J. M., Rodriquez, S., Sharma, S., Sheridan, P. J., Teinilä, K., Tuch, T., Viana, M., Virkkula, A., Weingartner, E., Wilhelm, R., and Wang, Y. Q.: Characterization

and intercomparison of aerosol absorption photometers: result of two intercomparison workshops, Atmospheric Measurement Techniques, 4, 245–268, https://doi.org/10.5194/amt-4-245-2011, publisher: Copernicus GmbH, 2011a.

Müller, T., Laborde, M., Kassell, G., and Wiedensohler, A.: Design and performance of a three-wavelength LED-based total scatter and backscatter integrating nephelometer, Atmospheric Measurement Techniques, 4, 1291–1303, https://doi.org/10.5194/amt-4-1291-2011, 2011b.

Nguyen, P. D. M., Martinussen, N., Mallach, G., Ebrahimi, G., Jones, K., Zimmerman, N., and Henderson, S. B.: Using Low-Cost Sensors to Assess Fine Particulate Matter Infiltration (PM2.5) during a Wildfire Smoke Episode at a Large Inpatient Healthcare Facility, International Journal of Environmental Research and Public Health, 18, 9811, https://doi.org/10.3390/ijerph18189811, number: 18 Publisher: Multidisciplinary Digital Publishing Institute, 2021.

Petzold, A., Ogren, J. A., Fiebig, M., Laj, P., Li, S.-M., Baltensperger, U., Holzer-Popp, T., Kinne, S., Pappalardo, G., Sugimoto, N., Wehrli, C., Wiedensohler, A., and Zhang, X.-Y.: Recommendations for reporting "black carbon" measurements, Atmospheric Chemistry and Physics, 13, 8365–8379, https://doi.org/10.5194/acp-13-8365-2013, publisher: Copernicus GmbH, 2013.

Rajesh, T. A. and Ramachandran, S.: Characteristics and source apportionment of black carbon aerosols over an urban site, Environmental Science and Pollution Research, 24, 8411–8424, https://doi.org/10.1007/s11356-017-8453-3, 2017.

Rajesh, T. A. and Ramachandran, S.: Black carbon aerosol mass concentration, absorption and single scattering albedo from single and dual spot aethalometers: Radiative implications, Journal of Aerosol Science, 119, 77–90, https://doi.org/10.1016/j.jaerosci.2018.02.001, publisher: Elsevier Ltd, 2018.

Rajesh, T. A., Ramachandran, S., and Dhaker, V. K.: Black carbon aerosols: Relative source strengths of vehicular emissions and residential/open wood burning over an urban and a semi-urban environment, Atmospheric Pollution Research, 12, 101 060, https://doi.org/10.1016/j.apr.2021.101060, 2021.

Sandradewi, J., Prévôt, A. S. H., Szidat, S., Perron, N., Alfarra, M. R., Lanz, V. A., Weingartner, E., and Baltensperger, U.: Using Aerosol Light Absorption Measurements for the Quantitative Determination of Wood Burning and Traffic Emission Contributions to Particulate Matter, Environmental Science & Technology, 42, 3316–3323, https://doi.org/10.1021/es702253m, publisher: American Chemical Society, 2008a.

Sandradewi, J., Prévôt, A. S. H., Weingartner, E., Schmidhauser, R., Gysel, M., and Baltensperger, U.: A study of wood burning and traffic aerosols in an Alpine valley using a multi-wavelength Aethalometer, Atmospheric Environment, 42, 101–112, https://doi.org/10.1016/j.atmosenv.2007.09.034, 2008b.

Schwarz, J. P., Gao, R. S., Fahey, D. W., Thomson, D. S., Watts, L. A., Wilson, J. C., Reeves, J. M., Darbeheshti, M., Baumgardner, D. G., Kok, G. L., Chung, S. H., Schulz, M., Hendricks, J., Lauer, A., Kärcher, B., Slowik, J. G., Rosenlof, K. H., Thompson, T. L., Langford, A. O., Loewenstein, M., and Aikin, K. C.: Single-particle measurements of midlatitude black carbon and light-scattering aerosols from the boundary layer to the lower stratosphere, Journal of Geophysical Research: Atmospheres, 111, https://doi.org/10.1029/2006JD007076, _eprint: https://onlinelibrary.wiley.com/doi/pdf/10.1029/2006JD007076, 2006.

Segura, S., Estellés, V., Titos, G., Lyamani, H., Utrillas, M. P., Zotter, P., Prévôt, A. S. H., Močnik, G., Alados-Arboledas, L., and Martínez-Lozano, J. A.: Determination and analysis of in situ spectral aerosol optical properties by a multi-instrumental approach, Atmospheric Measurement Techniques, 7, 2373–2387, https://doi.org/10.5194/amt-7-2373-2014, publisher: Copernicus GmbH, 2014.

Stampfer, O., Austin, E., Ganuelas, T., Fiander, T., Seto, E., and Karr, C. J.: Use of low-cost PM monitors and a multi-wavelength aethalometer to characterize PM2.5 in the Yakama Nation reservation, Atmospheric Environment, 224, 117 292, https://doi.org/10.1016/j.atmosenv.2020.117292, 2020.

https://doi.org/10.5194/amt-2022-278
Preprint. Discussion started: 4 November 2022

Szopa, S., Naik, V., Adhikary, B., Artaxo, P., Berntsen, T., Collins, W. D., Fuzzi, S., Gallardo, L., Kiendler-Scharr, A., and Klimont, Z.: Short-lived climate forcers Climate Change 2021: The Physical Science Basis. Contribution of Working Group I to the Sixth Assessment Report of the Intergovernmental Panel on Climate Change ed V Masson-Delmotte et al, 2021.

Tasoglou, A., Subramanian, R., and Pandis, S. N.: An inter-comparison of black-carbon-related instruments in a laboratory study of biomass burning aerosol, Aerosol Science and Technology, 52, 1320–1331, https://doi.org/10.1080/02786826.2018.1515473, publisher: Taylor & Francis, 2018.

Vecchi, R., Bernardoni, V., Paganelli, C., and Valli, G.: A filter-based light-absorption measurement with polar photometer: Effects of sampling artefacts from organic carbon, Journal of Aerosol Science, 70, 15–25, https://doi.org/10.1016/j.jaerosci.2013.12.012, 2014.

Virkkula, A., Mäkelä, T., Hillamo, R., Yli-Tuomi, T., Hirsikko, A., Hämeri, K., and Koponen, I. K.: A Simple Procedure for Correcting Loading Effects of Aethalometer Data, Journal of the Air & Waste Management Association, 57, 1214–1222, https://doi.org/10.3155/1047-3289.57.10.1214, 2007.

Virkkula, A., Chi, X., Ding, A., Shen, Y., Nie, W., Qi, X., Zheng, L., Huang, X., Xie, Y., Wang, J., Petäjä, T., and Kulmala, M.: On the interpretation of the loading correction of the aethalometer, Atmospheric Measurement Techniques, 8, 4415–4427, https://doi.org/10.5194/amt-8-4415-2015, publisher: Copernicus GmbH, 2015.

Wang, J. M., Jeong, C.-H., Hilker, N., Shairsingh, K. K., Healy, R. M., Sofowote, U., Debosz, J., Su, Y., McGaughey, M., Doerksen, G., Munoz, T., White, L., Herod, D., and Evans, G. J.: Near-Road Air Pollutant Measurements: Accounting for Inter-Site Variability Using Emission Factors, Environmental Science & Technology, 52, 9495–9504, https://doi.org/10.1021/acs.est.8b01914, publisher: American Chemical Society, 2018.

Wang, Q., Liu, H., Ye, J., Tian, J., Zhang, T., Zhang, Y., Liu, S., and Cao, J.: Estimating Absorption Ångström Exponent of Black Carbon Aerosol by Coupling Multiwavelength Absorption with Chemical Composition, Environmental Science & Technology Letters, 8, 121–127, https://doi.org/10.1021/acs.estlett.0c00829, publisher: American Chemical Society, 2021.

Weichenthal, S., Van Ryswyk, K., Kulka, R., Sun, L., Wallace, L., and Joseph, L.: In-Vehicle Exposures to Particulate Air Pollution in Canadian Metropolitan Areas: The Urban Transportation Exposure Study, Environmental Science & Technology, 49, 597–605, https://doi.org/10.1021/es504043a, publisher: American Chemical Society, 2015.

Weingartner, E., Saathoff, H., Schnaiter, M., Streit, N., Bitnar, B., and Baltensperger, U.: Absorption of light by soot particles: determination of the absorption coefficient by means of aethalometers, Journal of Aerosol Science, 34, 1445–1463, https://doi.org/10.1016/S0021-8502(03)00359-8, 2003.

WHO: Health effects of black carbon, WHO, 2012.

Wickham, H., Averick, M., Bryan, J., Chang, W., McGowan, L. D., François, R., Grolemund, G., Hayes, A., Henry, L., Hester, J., Kuhn, M., Pedersen, T. L., Miller, E., Bache, S. M., Müller, K., Ooms, J., Robinson, D., Seidel, D. P., Spinu, V., Takahashi, K., Vaughan, D., Wilke, C., Woo, K., and Yutani, H.: Welcome to the Tidyverse, Journal of Open Source Software, 4, 1686, https://doi.org/10.21105/joss.01686, 2019.

Zambrano-Bigiarini, M.: hzambran/hydroGOF: v0.4-0, https://doi.org/10.5281/ZENODO.839854, 2020.

Zotter, P., Herich, H., Gysel, M., El-Haddad, I., Zhang, Y., Močnik, G., Hüglin, C., Baltensperger, U., Szidat, S., and Prévôt, A. S. H.: Evaluation of the absorption Ångström exponents for traffic and wood burning in the Aethalometer-based source apportionment using radiocarbon measurements of ambient aerosol, Atmospheric Chemistry and Physics, 17, 4229–4249, https://doi.org/10.5194/acp-17-4229-2017, publisher: Copernicus GmbH, 2017.